Electronic Supplementary Material (ESI) for Inorganic Chemistry Frontiers.

Supporting Information

Construction of Multi-hydroxyl/ketone Lanthanide Metal-organic Frameworks for Understanding Mechanochromic Luminescence and High Proton Conductivity

Baoshan Hou,[†,§] Shuyi Yang,[†,§] Bo Li,[†] Guangfu Li,[†] Haiyan Zheng,[†] Chao Qin,[†] Guogang Shan,[†] Zhongmin Su,[†,‡] and Xinlong Wang*[,†,‡]

[†] College of Chemistry, Northeast Normal University, Changchun, China.

[‡] College of Science, Hainan University, Haikou, China

E-mail: wangxl824@nenu.edu.cn

[§]These authors contributed equally to this work.

General Experimental Section

Metal salts and solvents were obtained from commercial sources and used directly without further treatment. PXRD patterns were recorded on a Siemens D5005 diffractometer with Cu K*α* (*λ* = 1.5418 Å) ranging from 5 to 50º at room temperature. FT−IR spectrum was recorded on a Alpha Centaurt FT/IR spectrophotometer in the range 4000–400 cm^{-1} using KBr pellets. Diffuse reflectivity was performed on a Varian Cary 500 UV-vis spectrophotometer from 200 to 2000 nm using barium sulfate ($BaSO_4$) as a standard with 100% reflectance. TG curves were recorded on Perkin–Elmer TG–7 analyzer from room temperature to 800 ºC under nitrogen at the heating rate of 10 °C·min^{-1}. Solid-state fluorescence spectra were examined by an Edinburgh FLS920 phosphorimeter. equipped with a xenon lamp at room temperature.

Synthesis of [Zr_{16}-Eu]

The crystals of [Zr_{16}] (20mg), and $Eu(NO_3)_3·5H_2O$ (20 mg) were put in DMF (4 mL). The mixture was heated at 80 ºC for 12 h. The colorless crystals were collected by filtration and washed with fresh DMF 3 times. Elemental analysis (%): calculated for $[Zr_{16}Ln(SQA)_{11}(HSQA)_5(\mu_3\text{-}OH)_{12}(\mu_3\text{-}O)_4(\mu_2\text{-}O)_8(COO)_4\ (DMF)_{12}]$ 6DMF·29H_2O, C 25.24, H 3.53, N 4.34; found, C 26.18, H 3.85, N 4.58. FT-IR (KBr, 4000-400 cm^{-1}): 2927 (m), 1664 (s), 1602 (vs), 1508(s), 1249 (vs),1103 (m), 1058 (m), 890 (s), 754 (s), 628 (s), 505 (s).

Synthesis of [Zr_{16}-$Eu_{1-x}Tb_x$]

The Eu/Tb mixed MOFs **[Zr_{16}-$Eu_{1-x}Tb_x$]** were synthesized by using a mixture of $Eu(NO_3)_3·5H_2O$/$Tb(NO_3)_3·5H_2O$ (corresponding mole ratios) as the metal source through the same procedures.

Synthesis of [Zr_{16}-BPDC-Eu]

The crystals of [Zr_{16}] (20mg), $Eu(NO_3)_3·5H_2O$ (20 mg) and BPDC (20 mg) were put in DMF (4 mL). The mixture was heated at 80 ºC for 12 h. The colorless crystals were collected by filtration and washed with fresh DMF 3 times.

Synthesis of [Zr_{16}-BPDC-$Eu_{1-x}Tb_x$]

The Eu/Tb mixed MOFs **[Zr_{16}-BPDC-$Eu_{1-x}Tb_x$]** were synthesized by using a mixture of $Eu(NO_3)_3·5H_2O$/$Tb(NO_3)_3·5H_2O$ (corresponding mole ratios) as the metal source through the same procedures.

X−Ray structural determination

Bruker D8–Venture diffractometer with a Turbo X−ray Source (Cu *Kα* radiation, *λ* = 1.5418 Å) was used to collect the crystallographic data. The crystal structures were solved by using the Olex 2 software by the full matrix least−squares method.[28] The residual solvent molecules were removed using the SQUEEZE routine of PLATON program.[29] The DFIX, SIMU, ISOR instructions were used to make the structures more reasonable. The crystallographic data are provided in Table S1. The CCDC numbers are 2171770.

Proton conductivity measurement

The samples were grounded into uniform powders using a mortar and pestle. The powders were then put into a mold with an internal diameter of 10 mm and pressed into thin pellets

at 20 MPa for 30 seconds. The tablets were sandwiched by two gold-plated electrodes, and their thicknesses were about 0.6 mm, which were measured by a Vernier caliper. The proton conductivities of these two compounds were measured by the IviumStat electrochemical workstation (Netherland) using AC impedance measurements, and the test frequency ranged from 1 Hz to 1 MHz under an applied voltage of 50 mV. The temperature and relative humidity were controlled using a programmable SHHJ-ST-250 incubator. For the variable temperature electrochemical impedance (EIS) test, the thermal equilibrium was maintained for half an hour at each temperature condition, and the humidity equilibrium was maintained for 24 hours under each humidity condition. Use Zview software to fit the impedance data. The formula for calculating ionic conductivity with resistance is as follows:

$$\sigma = l/AR, \quad (1)$$

where σ represents the ionic conductivity (S cm^{-1}), l is the thickness, A is the cross-sectional area (cm^2) and R is the bulk resistance (Ω) of the sample. The activation energy was calculated by the transformation of the following formula:

$$\sigma T = \sigma_0 \exp(-Ea/k_B T), \quad (2)$$

where σ_0 represents the pre-exponential factor, k_B is the Boltzmann constant and T is the temperature.

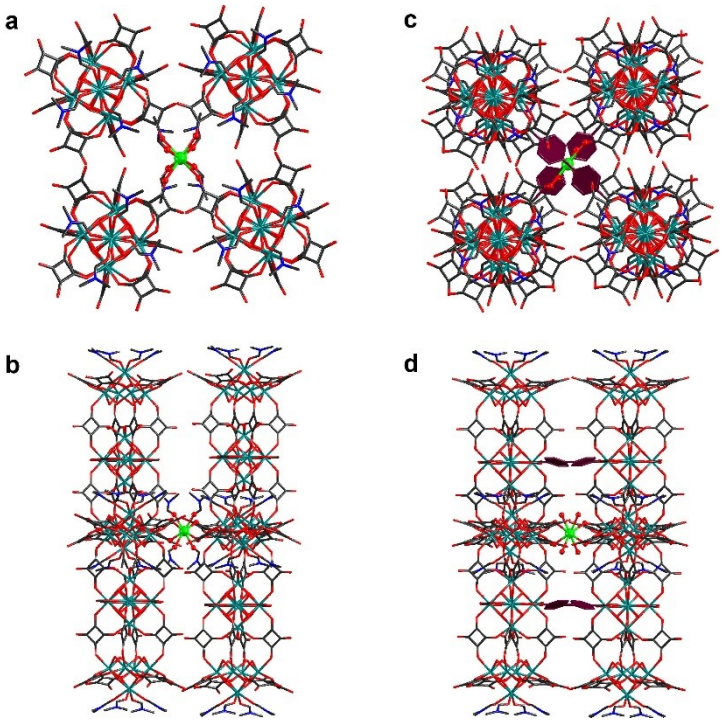

Figure S1 Coordination mode of Eu^{3+} ions in **[Zr_{16}-Eu]**(a,b) and **[Zr_{16}-BPDC-Eu]** (c,d).

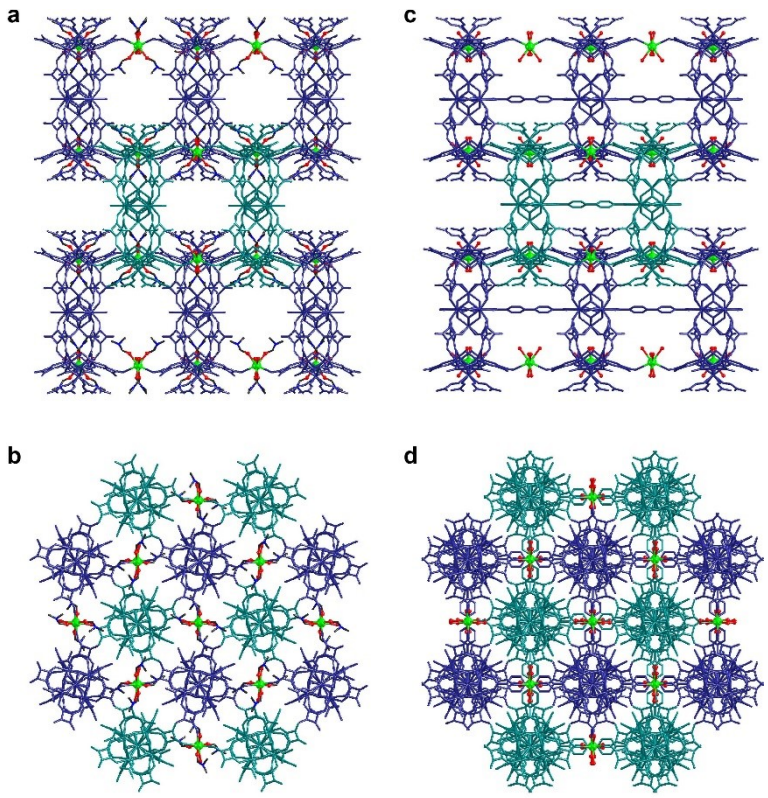

Figure S2 The packing structures of **[Zr_{16}-Eu]** (a,b) and **[Zr_{16}-BPDC-Eu]** (c,d).

Table S1 The Crystallographic data for **[Zr_{16}-Eu]**

Compound	**[Zr_{16}-Eu]**
Empirical formula	$C_{104}H_{88}EuN_{12}O_{108}Zr_{16}$
Formula weight	4845.34
Crystal system	Tetragonal
Space group	P4/mnc
Temperature (K)	293
Wavelength (Å)	1.54178 A
a (Å)	18.5785(8)
b (Å)	18.5785(8)
c (Å)	33.438(3)
α (°)	90
β (°)	90
γ (°)	90
Volume ($Å^3$)	11541.4(15)

Z	2
ρcalc. /g·cm^{-3}	1.394
μ/mm-1	8.303
F(000)	4726.0
Limiting indices	-19 ≤ h ≤ 21, -21 ≤ k ≤ 21, -38 ≤ l ≤ 38
Theta range for data collection (°)	2.643 to 63.684
Reflections collected	29765
Independent reflections	4836 [R(int) = 0.1137, R(sigma) = 0.0723]
Refinement method	Full-matrix least-squares on F^2
Data / restraints / parameters	4836/632/308
Goodness-of-fit on F^2	1.072
Final R indices [I > 2sigma(I)]	R_1 = 0.1659, wR_2 = 0.3650
R indices (all data)	R_1 = 0.2082, wR_2 = 0.3937

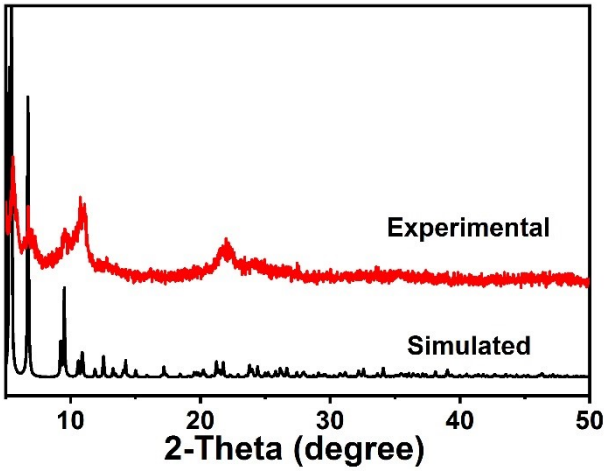

Figure S3 Simulated and experimental PXRD pattern of **[Zr_{16}-Eu]**.

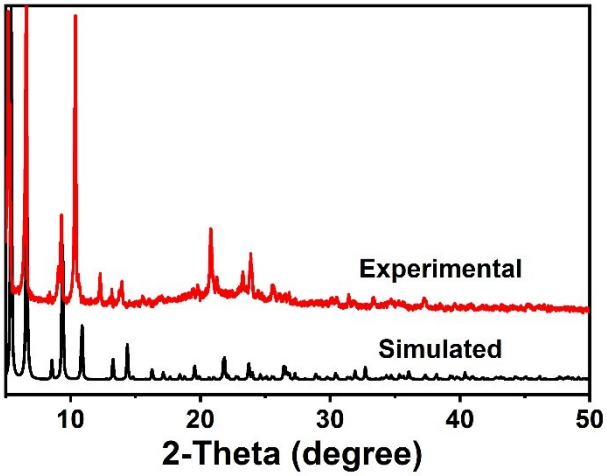

Figure S4 Simulated and experimental PXRD pattern of **[Zr_{16}-BPDC-Eu]**.

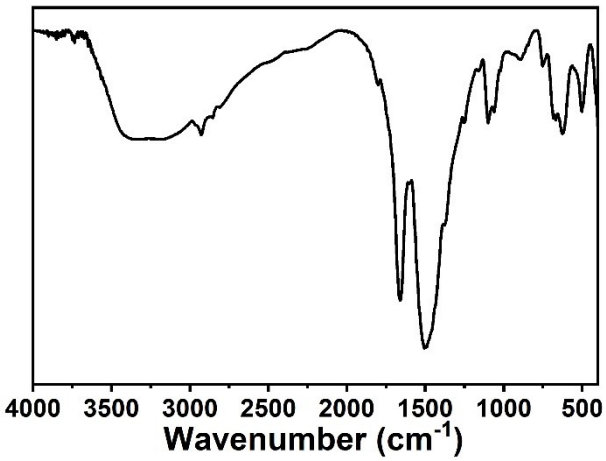

Figure S5 IR curves of **[Zr_{16}-Eu]**.

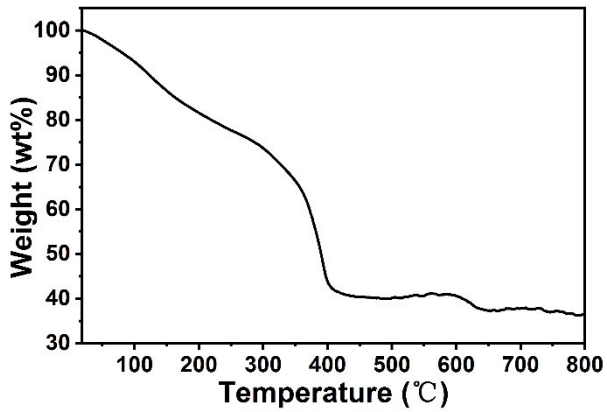

Figure S6 TG curves of **[Zr_{16}-Eu]**.

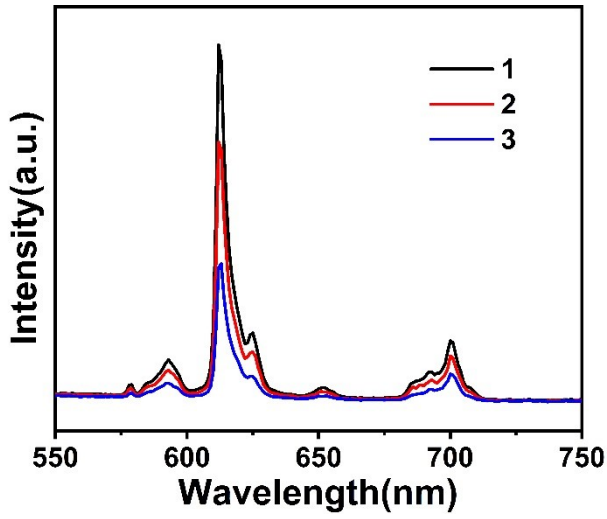

Figure S7 Change of the characteristic emission when grinding was applied: 1, **[Zr_{16}-Eu]** (black solid line); 2, first grinding (red solid line); 3, second grinding (blue solid line).

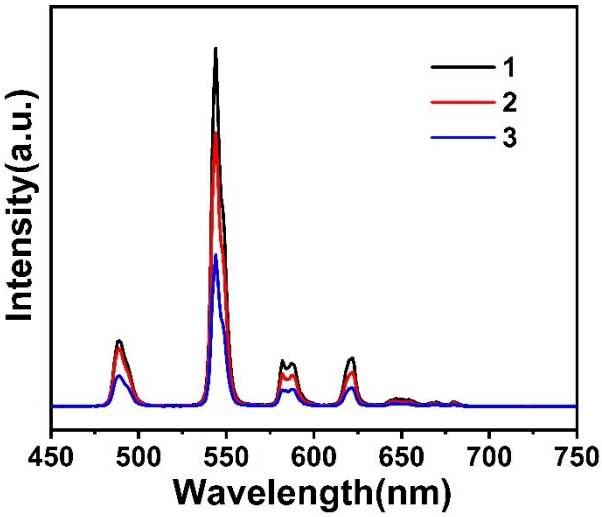

Figure S8 Change of the characteristic emission when grinding was applied: 1, **[Zr_{16}-Tb]** (black solid line); 2, first grinding (red solid line); 3, second grinding (blue solid line).

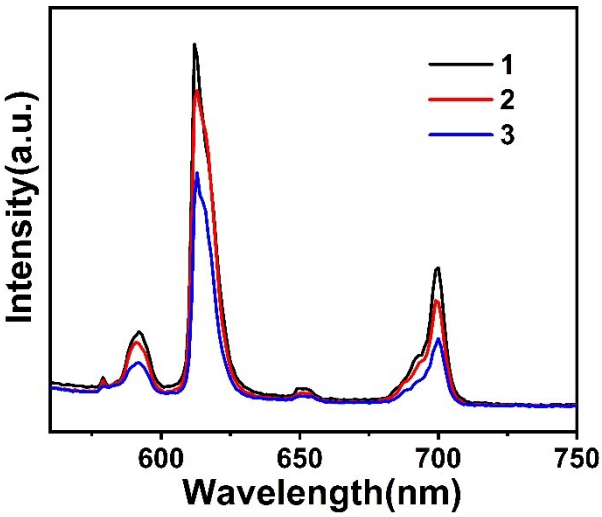

Figure S9 Change of the characteristic emission when grinding was applied: 1, **[Zr_{16}-BPDC-Eu]** (black solid line); 2, first grinding (red solid line); 3, second grinding (blue solid line).

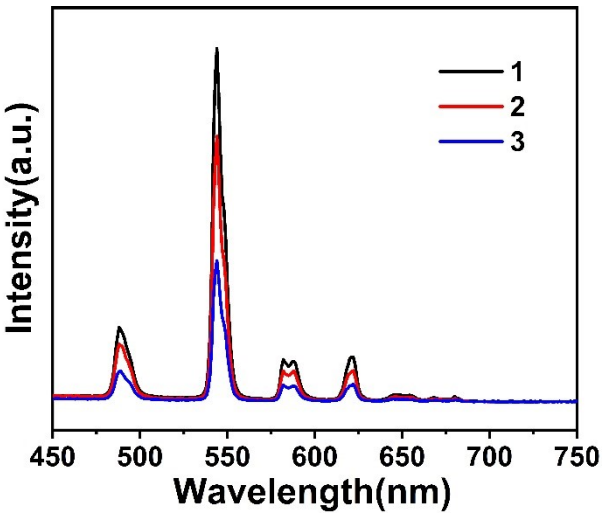

Figure S10 Change of the characteristic emission when grinding was applied: 1, **[Zr_{16}-BPDC-Tb]** (black solid line); 2, first grinding (red solid line); 3, second grinding (blue solid line).

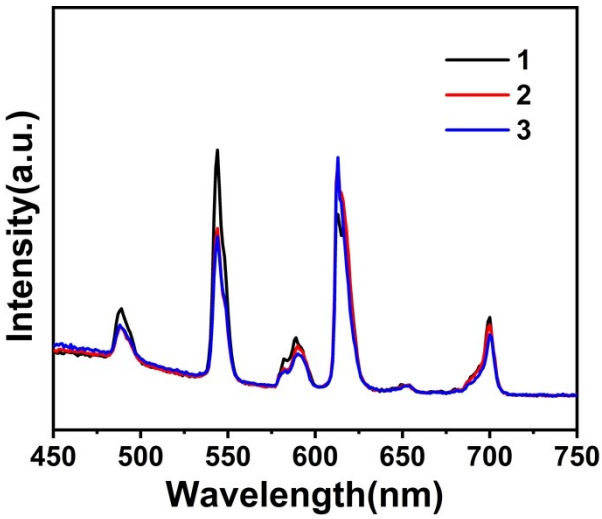

Figure S11 Change of the characteristic emission when grinding was applied: 1, **[Zr_{16}-BPDC-$Eu_{0.83}Tb_{0.17}$]** (black solid line); 2, first grinding (red solid line); 3, second grinding (blue solid line).

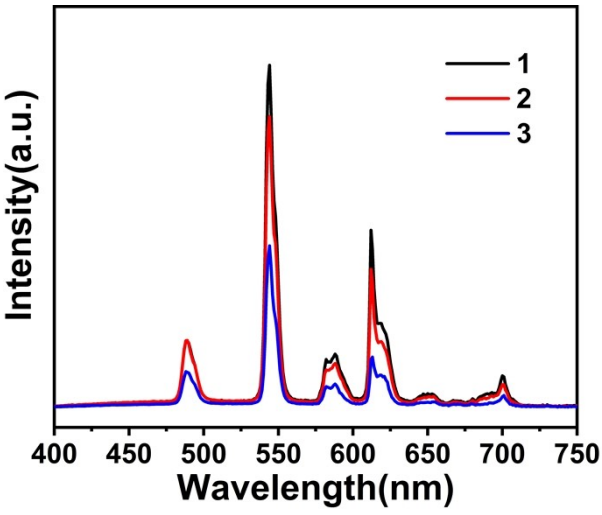

Figure S12 Change of the characteristic emission when grinding was applied: 1, **[Zr_{16}-$Eu_{0.83}Tb_{0.17}$]** (black solid line); 2, first grinding (red solid line); 3, second grinding (blue solid line).

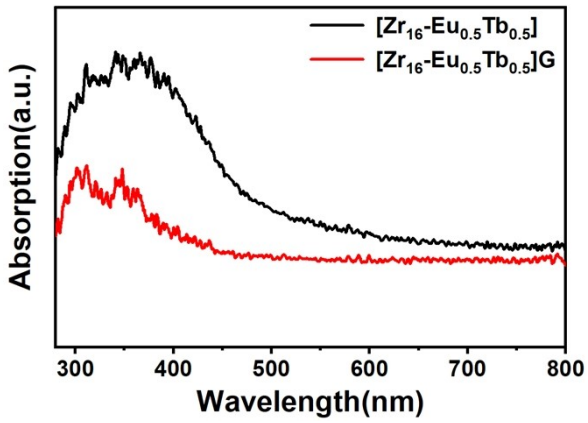

Figure S13 Solid UV–vis adsorption spectra of **[Zr_{16}-$Eu_{0.5}Tb_{0.5}$]** before and after grinding.

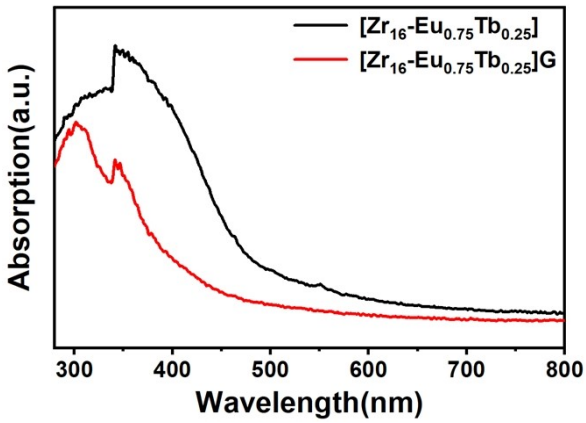

Figure S14 Solid UV–vis adsorption spectra of **[Zr_{16}- $Eu_{0.75}Tb_{0.25}$]** before and after grinding.

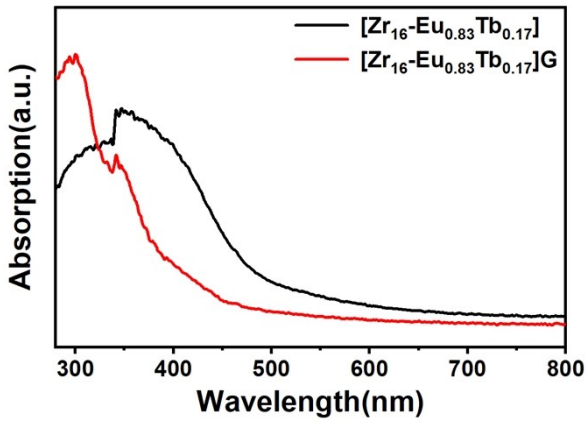

Figure S15 Solid UV–vis adsorption spectra of **[Zr_{16} -$Eu_{0.83}Tb_{0.17}$]** before and after grinding.

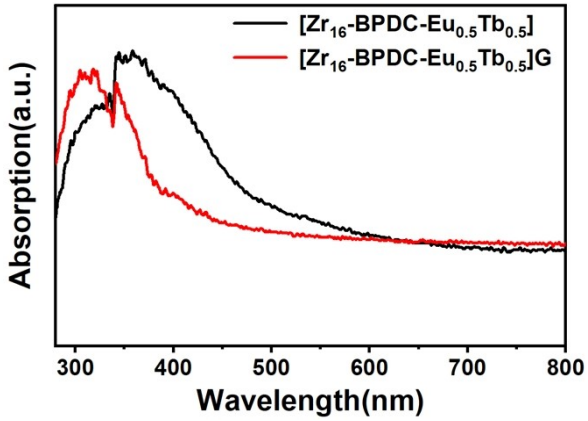

Figure S16 Solid UV–vis adsorption spectra of **[Zr_{16}-BPDC-$Eu_{0.5}Tb_{0.5}$]** before and after grinding.

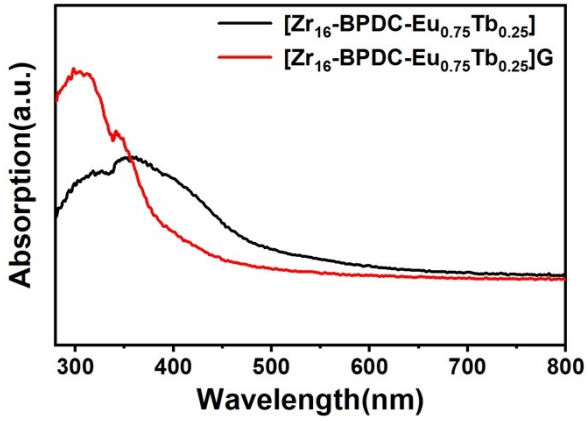

Figure S17 Solid UV–vis adsorption spectra of **[Zr_{16}-BPDC-$Eu_{0.75}Tb_{0.25}$]** before and after grinding.

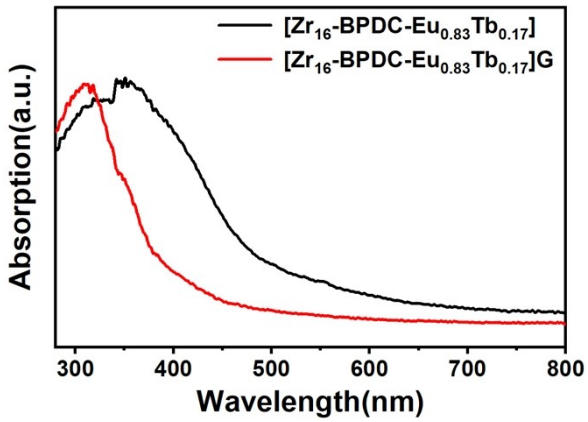

Figure S18 Solid UV–vis adsorption spectra of **[Zr_{16}-BPDC-$Eu_{0.83}Tb_{0.17}$]** before and after grinding.

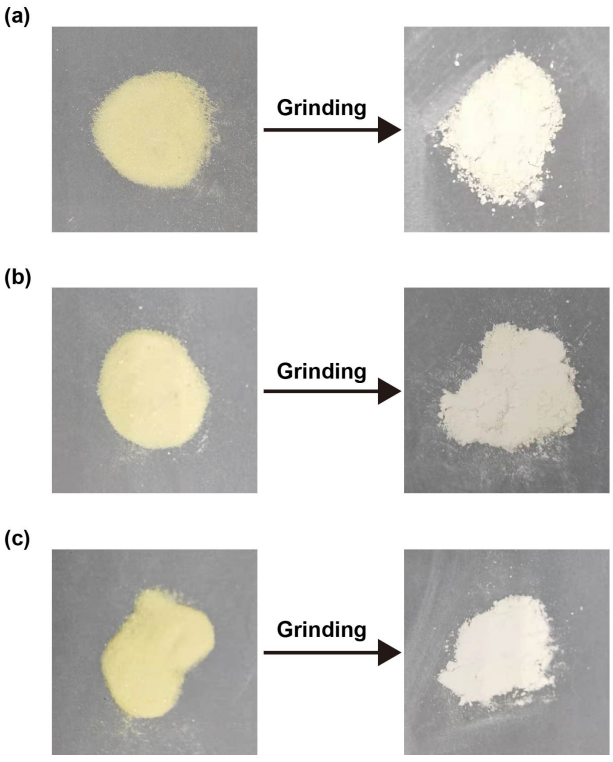

Figure S19 The color of **[Zr_{16}-$Eu_{0.5}Tb_{0.5}$](a), [Zr_{16}-$Eu_{0.75}Tb_{0.25}$] (b)** and **[Zr_{16}-$Eu_{0.83}Tb_{0.17}$] (c)** before and after grinding under room light.

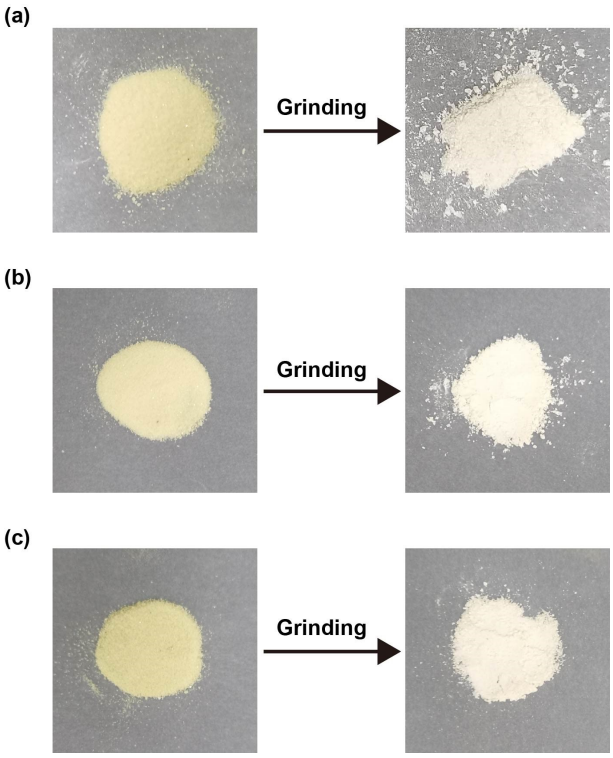

Figure S20 The color of **[Zr_{16}-BPDC-$Eu_{0.5}Tb_{0.5}$](a), [Zr_{16}-BPDC-$Eu_{0.75}Tb_{0.25}$] (b)** and **[Zr_{16}-BPDC-$Eu_{0.83}Tb_{0.17}$] (c)** before and after grinding under room light.

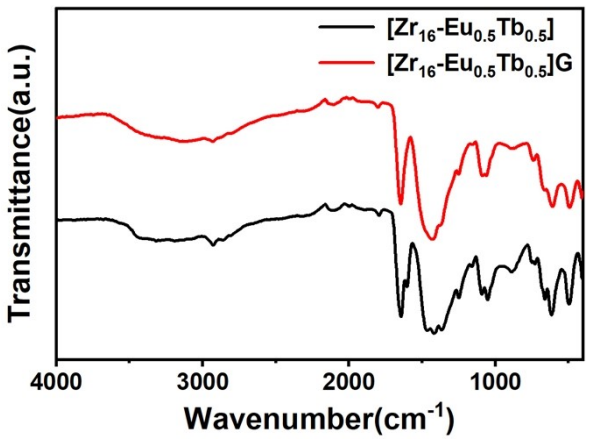

Figure S21 FT-IR spectra of **[Zr_{16}-$Eu_{0.5}Tb_{0.5}$]** before and after grinding.

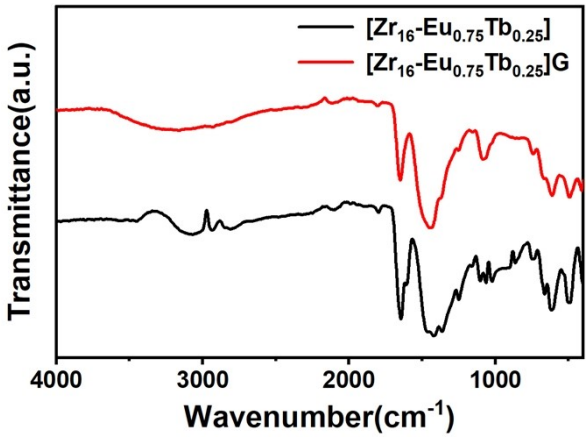

Figure S22 FT-IR spectra of **[Zr_{16}-$Eu_{0.75}Tb_{0.25}$]** before and after grinding.

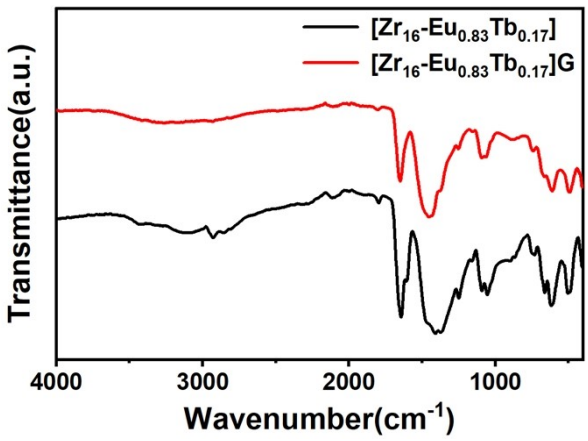

Figure S23 FT-IR spectra of **[Zr_{16}-$Eu_{0.83}Tb_{0.17}$]** before and after grinding.

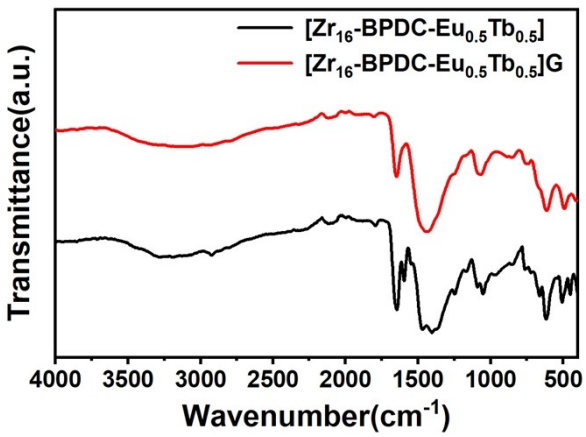

Figure S24 FT-IR spectra of **[Zr_{16}-BPDC-$Eu_{0.5}Tb_{0.5}$]** before and after grinding.

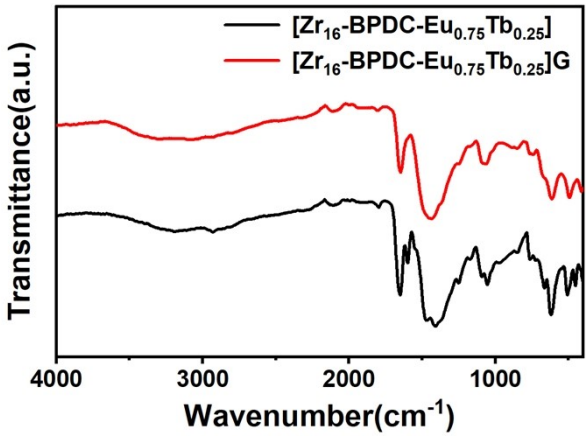

Figure S25 FT-IR spectra of **[Zr_{16}-BPDC-$Eu_{0.75}Tb_{0.25}$]** before and after grinding.

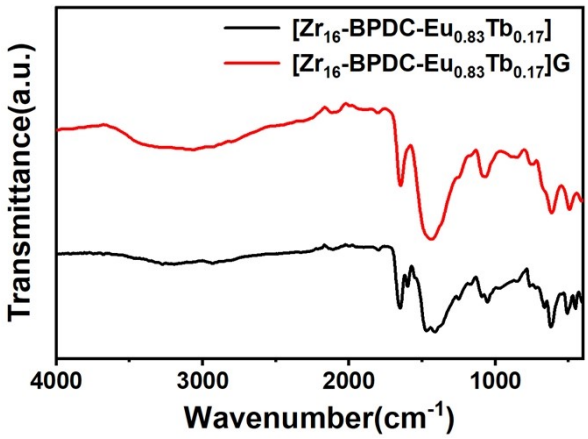

Figure S26 FT-IR spectra of **[Zr_{16}-BPDC-$Eu_{0.83}Tb_{0.17}$]** before and after grinding.

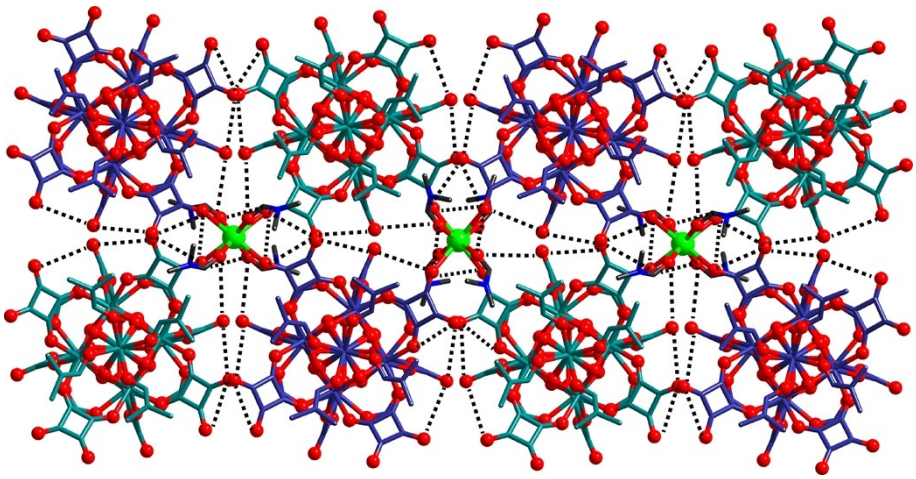

Figure S27 A schematic representation of the H-bonding network formed that is responsible for the proton conduction of **[Zr_{16}-Eu]**.

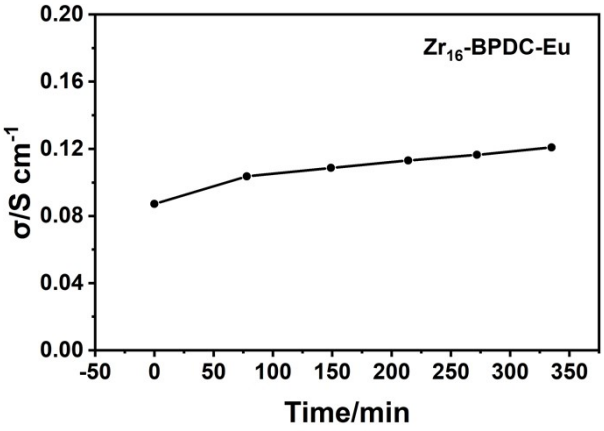

Figure S28 Time-dependent proton conductivity of **[Zr_{16}-BPDC-Eu]** measured at 303K and 97% relative humidity.

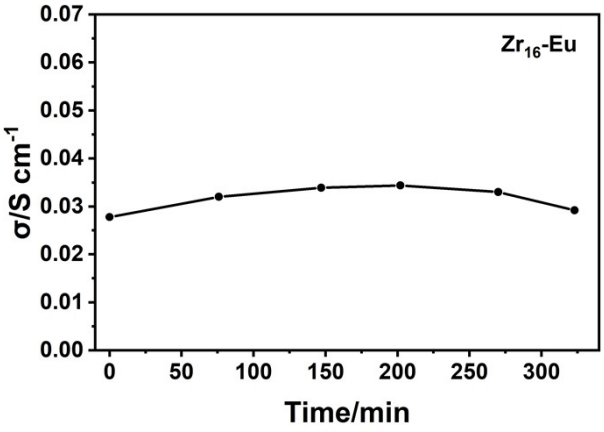

Figure S29 Time-dependent proton conductivity of **[Zr_{16}- Eu]** measured at 303K and 97% relative humidity.